$CeNi_{1-x}Sb_{1+y}Bi_{1-y}$ Phases with ZrCuSiAs-type and $CeNi_{1.26}Sb_2$ with $CaBe_2Ge_2$-type Structure

Konrad Schäfer, Birgit Gerke, Oliver Niehaus, and Rainer Pöttgen

Institut für Anorganische und Analytische Chemie, Universität Münster, Corrensstrasse 30, 48149 Münster, Germany

Reprint requests to R. Pöttgen. E-mail: pottgen@uni-muenster.de

Z. Naturforsch. **2014**, *69b*, 409 – 416 / DOI: 10.5560/ZNB.2014-4018
Received February 5, 2014

Block- and platelet-shaped single crystals of several $CeNi_{1-x}Sb_{1+y}Bi_{1-y}$ phases with ZrCuSiAs-type structure (space group $P4/nmm$) were grown from a CeNiSb precursor in bismuth fluxes. The structures of $CeNiSb_{1.19}Bi_{0.81}$, $CeNi_{0.80}Sb_{1.16}Bi_{0.84}$ and $CeNi_{0.75}Sb_{1.74}Bi_{0.26}$ were refined from single-crystal X-ray diffractometer data. The 2*b* nickel site can be fully or partially occupied, and the bismuth square nets show solid solutions with antimony. $CaBe_2Ge_2$-type $CeNi_{2-x}Sb_2$ crystals occur as by-products of the crystal growth experiments. The structure of a $CeNi_{1.26}Sb_2$ crystal has been refined. The small difference of the compositions hamper phase analytical studies by powder X-ray diffraction. A polycrystalline CeNiSbBi sample showed Curie-Weiss behavior with an experimental magnetic moment of 2.56(1) μ_B per Ce atom, indicating purely trivalent cerium. No magnetic ordering is detected down to 2.5 K. A ^{121}Sb Mössbauer spectrum showed an isomer shift of $\delta = -8.06(6)$ mm s^{-1}, substantiating the antimonide character.

Key words: Antimonide, Bismuthide, Crystal Structure, Intermetallics

Introduction

The equiatomic tetrelides Ce*TX* (*T* = electron-rich transition metal; *X* = Si, Ge, Sn) show hydrogen insertion up to compositions $CeTXH_{1.8}$ [1, 2]. The hydrogen atoms fill tetrahedral sites and strongly influence the electronic structure along with the magnetic ground state. To give an example, intermediate-valent Ce in CeRhSn transforms to almost trivalent Ce in $CeRhSnH_{0.8}$ [3] and the hydride $CeNiSiH_{0.8}$ shows a higher Kondo effect than CeNiSi [4]. These studies have been extended to the equiatomic pnictides. A tiny amount of hydrogen leads to the formation of $CeRhSbH_{0.2}$ [5], and one observes a change from valence fluctuations in CeRhSb to antiferromagnetic ordering at 3.6 K in the hydride.

In continuation of these studies we were interested in the hydrogenation behavior of the ferromagnetic Kondo lattice compound CeNiSb. So far, this antimonide had only been characterized on the basis of powder diffraction data [6 – 13]. Since some nickel-antimony disorder was evident from powder neutron diffraction [9], we tried the growth of small single crystals by standard annealing techniques, however, without success. Subsequent flux growth experiments in liquid bismuth [14 – 16] led to the new quaternary pnictides $CeNi_{1-x}Sb_{1+y}Bi_{1-y}$ (in this case bismuth acts as a reactive flux medium). These can be considered as solid solutions of $CeNi_{1-x}Sb_2$ [17 – 20] with $CeNi_{1-x}Bi_2$ [21, 22]. This field of research gained new input when superconductivity at ~4 K was observed for $CeNi_{0.8}Bi_2$ [23, 24], induced by the nickel defects. The transition to superconductivity has also been observed for epitaxially grown thin films [25].

Herein we report on single-crystal X-ray data of the $CeNi_{1-x}Sb_{1+y}Bi_{1-y}$ phases with respect to antimony-bismuth ordering as well as on magnetic and ^{121}Sb Mössbauer spectroscopic data of polycrystalline CeNiSbBi and a structure refinement of $CeNi_{1.26}Sb_2$ with a defect $CaBe_2Ge_2$-type structure.

Experimental

Synthesis

Single crystals of $CeNiSb_{1.19}Bi_{0.81}$, $CeNi_{0.80}Sb_{1.16}Bi_{0.84}$ and $CeNi_{0.75}Sb_{1.74}Bi_{0.26}$ were synthesized with polycrystalline CeNiSb as precursor compound. This precursor was mixed with Bi powder in an atomic ratio of 1 : 40, ground

in an agate mortar and cold-pressed to pellets of 6 mm diameter. The pellets were sealed in evacuated quartz ampoules and placed in muffle furnaces. They were heated at a rate of 10 K h^{-1} to 1170 K and kept at that temperature for 14 d. Then the samples were cooled at a rate of 20 K h^{-1} to room temperature. The bismuth flux was dissolved in a 1 : 1 mixture of H_2O_2 (Across, 35 %) and glacial acetic acid (VWR International, 96 %). $CeNi_{2-x}Sb_2$ crystals were obtained as by-product in several samples.

Starting materials for the synthesis of the polycrystalline samples were cerium ingots (Sigma Aldrich), nickel (Merck), antimony (Johnson Matthey) and bismuth (Sigma Aldrich) powder, all with stated purities better than 99.9 %. Filings of cerium were prepared under paraffin oil, washed with cyclohexane (both dried over sodium wire) and kept in Schlenk tubes prior to the reactions. The elements were mixed in a mortar, subsequently cold-pressed to pellets of 6 mm diameter and sealed in evacuated quartz tubes. The ampoules were heated in muffle furnaces up to 620 K within 48 h and kept at that temperature for 48 h. In the next step the samples were heated up to 1170 K within 96 h and kept at that temperature for another 14 d. Finally the samples were cooled down to room temperature over a period of 96 h. The resulting samples were ground, repressed to pellets and annealed again with the same sequence. The resulting samples are silvery with metallic luster. They are stable in air over a few days before slow hydrolyses starts.

EDX data

Semiquantitative EDX analyses of the single crystals studied on the diffractometer were carried out in the variable pressure mode with a Zeiss EVO® MA10 scanning electron microscope with CeF_3, Ni, Sb and Bi as standards. The experimentally observed average compositions were close to the ideal ones. No impurity elements heavier than sodium were detected.

X-Ray diffraction

The polycrystalline $CeNi_{1-x}Sb_{1+y}Bi_{1-y}$ samples were characterized by powder X-ray diffraction on a Guinier camera (equipped with a Fujifilm image plate system, BAS-1800) using Cu$K_{\alpha 1}$ radiation and α-quartz ($a = 491.30$, $c = 540.46$ pm) as an internal standard. The tetragonal lattice parameters (Table 1) of several samples with different starting compositions were refined from the powder data by a least-squares routine. The experimental powder patterns were compared to the calculated ones [26] in order to ensure correct indexing.

The $CeNi_{1-x}Sb_{1+y}Bi_{1-y}$ phases crystallize with two different crystal habits. Crystals with full nickel content form small blocks (Fig. 1), while the ones with a nickel deficit crystallize in the form of platelets. Diverse crystals were mechanically selected from the dissolved bismuth flux and glued to quartz fibers using bees wax. Their quality was first tested by Laue photographs on a Buerger camera (white Mo radiation; image plate detection system). Intensity data of the $CeNi_{1-x}Sb_{1+y}Bi_{1-y}$ crystals were collected at room temperature by use of a Stoe IPDS-II imaging plate diffractometer

Table 1. Refined lattice parameters (Guinier powder data) of the intermetallic compounds $CeNi_{1-x}Sb_{1+y}Bi_{1-y}$. Standard deviations are given in parentheses. The lattice parameters of $CaBe_2Ge_2$-type $CeNi_{2-x}Sb_2$ and $CeNi_{2-x}Bi_2$ are listed for comparison.

Compound	a (pm)	c (pm)	V (nm^3)
$CeNiSb_{2-x}Bi_x$ samples			
CeNiSbBi	445.2(1)	975.8(3)	0.1934
$CeNiSb_{1.2}Bi_{0.8}$	445.1(1)	976.3(3)	0.1934
$CeNiSb_{1.25}Bi_{0.75}$	445.0(1)	976.3(3)	0.1933
$CeNiSb_{1.4}Bi_{0.6}$	444.2(1)	975.7(3)	0.1925
$CeNiSb_{1.6}Bi_{0.4}$	439.8(1)	974.0(3)	0.1884
$CeNiSb_{1.8}Bi_{0.2}$	441.0(1)	973.9(4)	0.1894
$CeNiSb_2$	438.0(2)	973.8(4)	0.1868
$CeNiSb_2$ [18]	439.3(1)	975.0(3)	0.1882
$CeNiSb_{1.95}$ [19]	440.3	976.1	0.1892
$CeNi_{2-x}Sb_2$ [21]	441.3(1)	984.6(4)	0.1918
$CeNi_{1.26}Sb_2$	440.23(6)	976.1(2)	0.1892
$CeNiBi_2$ [22]	454.2(1)	963.8(3)	0.1988
$CeNi_{0.8}Bi_2$ [24]	454.4(1)	964.1(2)	0.1991
$CeNi_{2-x}Bi_2$ [21]	454.6(1)	965.6(3)	0.1996
$CeNi_{0.75}Sb_{2-x}Bi_x$ samples			
$CeNi_{0.75}Bi_2$	437.6(1)	969.4(6)	0.1856
$CeNi_{0.75}SbBi$	445.3(1)	973.1(3)	0.1930
$CeNi_{0.75}Sb_{1.25}Bi_{0.75}$	441.2(2)	976.1(6)	0.1900
$CeNi_{0.75}Sb_{1.4}Bi_{0.6}$	439.5(1)	962.3(3)	0.1859
$CeNi_{0.75}Sb_{1.5}Bi_{0.5}$	441.1(1)	975.3(2)	0.1898
$CeNi_{0.75}Sb_{1.75}Bi_{0.25}$	438.7(1)	971.8(3)	0.1870
$CeNi_{0.75}Sb_{1.8}Bi_{0.2}$	438.2(2)	972.8(4)	0.1868
$CeNi_{0.75}Sb_2$	438.1(1)	973.3(3)	0.1868

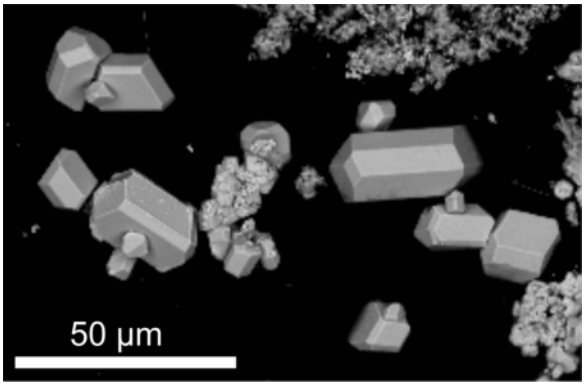

Fig. 1. Scanning electron micrograph of $CeNiSb_{1+x}Bi_{1-x}$ single crystals grown in a bismuth flux.

Table 2. Crystallographic data and structure refinement of $CeNiSb_{1.19}Bi_{0.81}$, $CeNi_{0.80}Sb_{1.16}Bi_{0.84}$, $CeNi_{0.75}Sb_{1.74}Bi_{0.26}$, and $CeNi_{1.26}Sb_2$, $P4/nmm$, $Z = 2$.

Empirical formula	$CeNiSb_{1.19}Bi_{0.81}$	$CeNi_{0.80}Sb_{1.16}Bi_{0.84}$	$CeNi_{0.75}Sb_{1.74}Bi_{0.26}$	$CeNi_{1.26}Sb_2$
Molar mass, g mol^{-1}	513.1	513.1	450.6	457.4
Unit cell dimensions (single crystal data)				
a, pm	445.68(3)	445.59(3)	440.09(3)	440.23(6)
c, pm	977.86(10)	972.68(10)	971.83(10)	976.1(2)
V, nm^3	0.1942	0.1931	0.1882	0.1892
Calculated density, g cm^{-3}	8.77	8.82	7.95	8.03
Crystal size, μm^3	$20 \times 40 \times 50$	$20 \times 50 \times 60$	$20 \times 30 \times 60$	$20 \times 20 \times 30$
Transm. ratio (max / min)	1.82	2.91	4.83	2.67
Absorption coefficient, mm^{-1}	60.8	61.2	40.0	32.6
Detector distance, mm	60	60	80	40
Exposure time, sec	180	600	180	20
ω-range / increment, deg	0 – 180 / 1.0	0 – 180 / 1.0	0 – 180 / 1.0	−60 to −2 / 0.5
Integrat. param. A / B / EMS	12.4 / 3.2 / 0.012	22.0 / 10.0 / 0,080	12.8 / 3.2 / 0,012	7.5 / 4.9 / 0,013
$F(000)$, e	428	419	379	390
θ-range for data collection, deg	4 – 36	5 – 34	4 – 35	4 – 40
Range in hkl	±7, ±7, ±16	±7, ±7, ±15	±7, ±7, ±15	±7, ±7, ±17
Total no. reflections	3232	2714	2924	6571
Independent reflections/R_{int}	311 / 0.0371	269 / 0.0368	283 / 0.0842	376 / 0.0431
Reflections with $I > 2\sigma(I)$	305	266	262	335
Data / parameter	311 / 12	269 / 12	283 / 14	376 / 17
Goodness-of-fit on F^2	2.12	1.27	2.74	1.24
$R1$ / $wR2$ für $I > 2\sigma(I)$	0.0237 / 0.0559	0.0163 / 0.0333	0.0274 / 0.0704	0.0151 / 0.0359
$R1/wR2$ (all data)	0.0241 / 0.0560	0.0165 / 0.0334	0.0306 / 0.0710	0.0188 / 0.0370
Extinction coefficient	500(30)	406(12)	130(30)	213(13)
Largest diff. peak / hole, e Å^{-3}	4.09/−2.59	1.21/−1.29	2.87/−4.76	1.41/−1.14

in oscillation mode (graphite-monochromatized MoK_α radiation). The $CeNi_{1.26}Sb_2$ crystal was measured on a Stoe StadiVari instrument equipped with a Mo microfocus source and a Pilatus 100 K Detector with a hybrid-pixel sensor. Numerical absorption corrections were applied to the data sets. All relevant details concerning the data collections and evaluations are listed in Table 2.

Structure refinements

The diffractometer data sets showed tetragonal lattices with high Laue symmetry, and the systematic extinctions were in agreement with the space group $P4/nmm$, similar to the ZrCuSiAs type [27]. The starting parameters were obtained with the SUPERFLIP algorithm [28] embedded in the JANA2006 program package [29]. The structures were refined with anisotropic displacement parameters for all atoms. Since the powder neutron diffraction data showed substantial nickel defects for $CeNi_{0.8}Bi_2$ [24], we refined the occupancy parameters of all nickel and antimony (bismuth) sites in order to check for deviations from the ideal composition. The first crystal showed full nickel occupancy, but a small degree of Bi/Sb mixing on the 2a position. The other two crystals also revealed nickel defects. These occupancy parameters were then refined as least-squares variables in the final cycles, leading to the compositions $CeNiSb_{1.19}Bi_{0.81}$, $CeNi_{0.80}Sb_{1.16}Bi_{0.84}$ and $CeNi_{0.75}Sb_{1.74}Bi_{0.26}$ for the investigated crystals. Furthermore we refined the structure of a $CaBe_2Ge_2$ type crystal, space group $P4/nmm$. Such crystals were observed as by-products. Similar to $LaNi_{1.51}Sb_2$ [21], the two nickel sites of the $CeNi_{1.26}Sb_2$ crystal also showed significant defects and the occupancy parameters were refined as least-squares variables in the last cycles. The final difference Fourier synthesis revealed no residual peaks. The refined atomic positions, displacement parameters, and interatomic distances are listed in Tables 3 and 4.

Further details of the crystal structure investigations may be obtained from Fachinformationszentrum Karlsruhe, 76344 Eggenstein-Leopoldshafen, Germany (fax: +49-7247-808-666; e-mail: crysdata@fiz-karlsruhe.de, http://www.fiz-karlsruhe.de/request_for_deposited_data.html) on quoting the deposition numbers CSD-427339 ($CeNiSb_{1.19}Bi_{0.81}$), CSD-427338 ($CeNi_{0.80}Sb_{1.16}Bi_{0.84}$), CSD-427337 ($CeNi_{0.75}Sb_{1.74}Bi_{0.26}$), and CSD-427340 ($CeNi_{1.26}Sb_2$).

Magnetic susceptibility measurements

Magnetic measurements of a CeNiSbBi sample were carried out on a Quantum Design Physical Property Measurement System using the Vibrating Sample Magnetometer option. For the measurement 26.312 mg of the powdered sam-

Table 3. Atomic coordinates and anisotropic displacement parameters (pm^2) for $CeNiSb_{1.19}Bi_{0.81}$, $CeNi_{0.80}Sb_{1.16}Bi_{0.84}$, $CeNi_{0.75}Sb_{1.74}Bi_{0.26}$, and $CeNi_{1.26}Sb_2$. U_{eq} is defined as one third of the trace of the orthogonalized U_{ij} tensor. $U_{12} = U_{13} = U_{23} = 0$.

Atom	Site	x	y	z	$U_{11} = U_{22}$	U_{33}	U_{eq}
$CeNiSb_{1.19}Bi_{0.81}$							
Ce	2*c*	1/4	1/4	0.26788(6)	59(2)	65(2)	61(1)
Ni	2*b*	3/4	1/4	1/2	185(6)	113(6)	161(3)
0.81(1)Bi1+0.19(1)Sb1	2*a*	3/4	1/4	0	75(2)	89(2)	80(1)
Sb2	2*c*	1/4	1/4	0.63207(8)	66(2)	130(3)	88(1)
$CeNi_{0.80}Sb_{1.16}Bi_{0.84}$							
Ce	2*c*	1/4	1/4	0.26913(4)	146(1)	137(2)	143(1)
0.80(1)Ni	2*b*	3/4	1/4	1/2	216(4)	156(5)	196(2)
0.84(1)Bi1+0.16(1)Sb1	2*a*	3/4	1/4	0	155(1)	166(1)	159(1)
Sb2	2*c*	1/4	1/4	0.63081(5)	142(2)	193(2)	159(1)
$CeNi_{0.75}Sb_{1.74}Bi_{0.26}$							
Ce	2*c*	1/4	1/4	0.26370(7)	106(3)	99(3)	104(2)
0.75(1)Ni	2*b*	3/4	1/4	1/2	174(9)	142(11)	164(6)
0.27(1)Bi1+0.73(1)Sb1	2*a*	3/4	1/4	0	125(3)	122(3)	124(2)
Sb2	2*c*	1/4	1/4	0.62856(8)	120(3)	161(4)	134(2)
$CeNi_{1.26}Sb_2$							
Ce	2*c*	1/4	1/4	0.73965(3)	147(1)	158(1)	151(6)
0.32(1)Ni1	2*c*	1/4	1/4	0.1155(3)	228(8)	177(10)	211(5)
0.94(1)Ni2	2*b*	3/4	1/4	1/2	242(3)	183(3)	223(2)
Sb1	2*c*	1/4	1/4	0.36964(4)	162(1)	217(2)	180(1)
Sb2	2*a*	3/4	1/4	0	235(1)	182(2)	218(1)

Table 4. Interatomic distances (pm) in the structures of $CeNiSb_{1.19}Bi_{0.81}$, $CeNi_{0.80}Sb_{1.16}Bi_{0.84}$, $CeNi_{0.75}Sb_{1.74}Bi_{0.26}$, and $CeNi_{1.26}Sb_2$. All distances of the first coordination spheres are listed. Standard deviations are all smaller or equal than 0.1 pm.

$CeNiSb_{1.19}Bi_{0.81}$				**$CeNi_{0.80}Sb_{1.16}Bi_{0.84}$**				**$CeNi_{1.26}Sb_2$**			
Ce:	4	Ni	318.1	Ce:	4	Ni	316.3	Ce:	4	Ni2	321.2
	4	Sb2	330.0		4	Sb2	329.8		4	Sb1	329.1
	4	Bi1/Sb1	343.9		4	Bi1/Sb1	343.8		4	Sb2	336.2
Ni:	4	Sb2	257.6	Ni:	4	Sb2	256.6	Ni1:	4	Sb2	247.3
	4	Ni	315.1		4	Ni	315.1		4	Ce	341.9
	4	Ce	318.1		4	Ce	316.3		1	Ce	366.8
Bi1/Sb1:	4	Bi1/Sb1	315.1	Bi1/Sb1:	4	Bi1/Sb1	315.1	Ni2:	4	Sb1	254.2
	4	Ce	343.9		4	Ce	343.8		4	Ni2	311.3
Sb2:	4	Ni	257.6	Sb2:	4	Ni	256.6		4	Ce	321.2
	4	Ce	330.0		4	Ce	329.8	Sb1:	1	Ni1	248.1
$CeNi_{0.75}Sb_{1.74}Bi_{0.26}$									4	Ni2	254.2
Ce:	4	Ni	318.1						4	Ce	329.1
	4	Sb2	328.3					Sb2:	4	Ni1	247.3
	4	Bi1/Sb1	337.8						4	Sb2	311.3
Ni:	4	Sb2	253.0						4	Ce	336.2
	4	Ni	311.2								
	4	Ce	318.1								
Sb1/Bi1:	4	Sb1/Bi1	311.2								
	4	Ce	337.8								
Sb2:	4	Ni	253.0								
	4	Ce	328.3								

ple was packed in a polypropylene capsule and attached to the sample holder rod. The measurements were performed in the temperature range of 2.5 – 300 K with magnetic flux densities up to 80 kOe (1 kOe = 7.96×10^4 A m^{-1}).

^{121}Sb Mössbauer spectroscopy

A $Ba^{121m}SnO_3$ source was used for the Mössbauer spectroscopic experiment, and the quoted values of the iso-

mer shift are given relative to this material. The measurement was carried out in the usual transmission geometry at 78 K. The temperature was controlled by a resistance thermometer (±0.5 K accuracy), and the Mössbauer source was kept at room temperature. The sample was enclosed in small PVC container at a thickness corresponding to about 10 mg Sb cm^{-2}. The total counting time was approximately 2 days. Fitting of the spectrum was performed with the NORMOS-90 program system [30].

Discussion

Crystal chemistry

The ternary and quaternary pnictides $CeNi_{1-x}Sb_{1+y}Bi_{1-y}$ crystallize with the ZrCuSiAs-type structure [27], space group $P4/nmm$, which is a quaternary, ordered version of the $HfCuSi_2$ structure [31, 32]. The unit cell for the ordered antimonide bismuthide CeNiSbBi is presented in Fig. 2. The many pnictide oxides *RETPn*O (*RE* = rare earth element; *T* = electron-rich transition metal; *Pn* = P, As, Sb) [33 – 35] crystallize with the same space group, and the atoms fill the same Wyckoff sites (sequence c^2ba), however, there are distinct differences in the lattice parameters and in the two free *z* parameters (especially those of the 2*c* *RE* sites), leading to differences in chemical bonding. One should call these compounds rather isopointal than isotypic [36, 37].

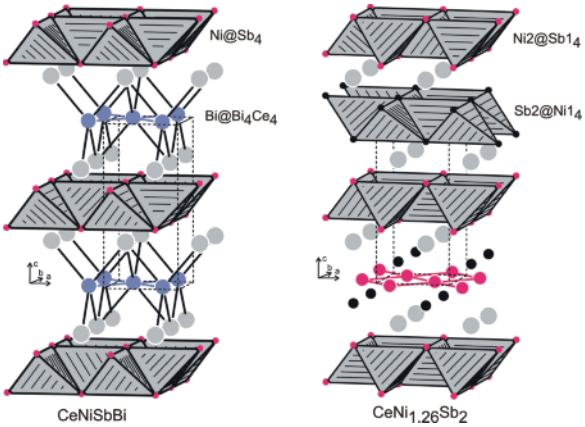

Fig. 2. (color online). The crystal structures of CeNiSbBi and $CeNi_{1.26}Sb_2$. The stackings of the tetrahedral layers are emphasized.

Another point that complicates analyses of the $CeNi_{1-x}Sb_{1+y}Bi_{1-y}$ phase is the close structural relationship with the tetragonal, $CaBe_2Ge_2$-type pnictides $CeNi_{2-x}Sb_2$ and $CeNi_{2-x}Bi_2$ [21]. These two phases also crystallize with space group $P4/nmm$ with an additional partially occupied nickel site. The lattice parameters are in the same range and the powder X-ray patterns show small differences in their intensities (Fig. 3). Thus, single-crystal data are an important prerequisite for structural investigation.

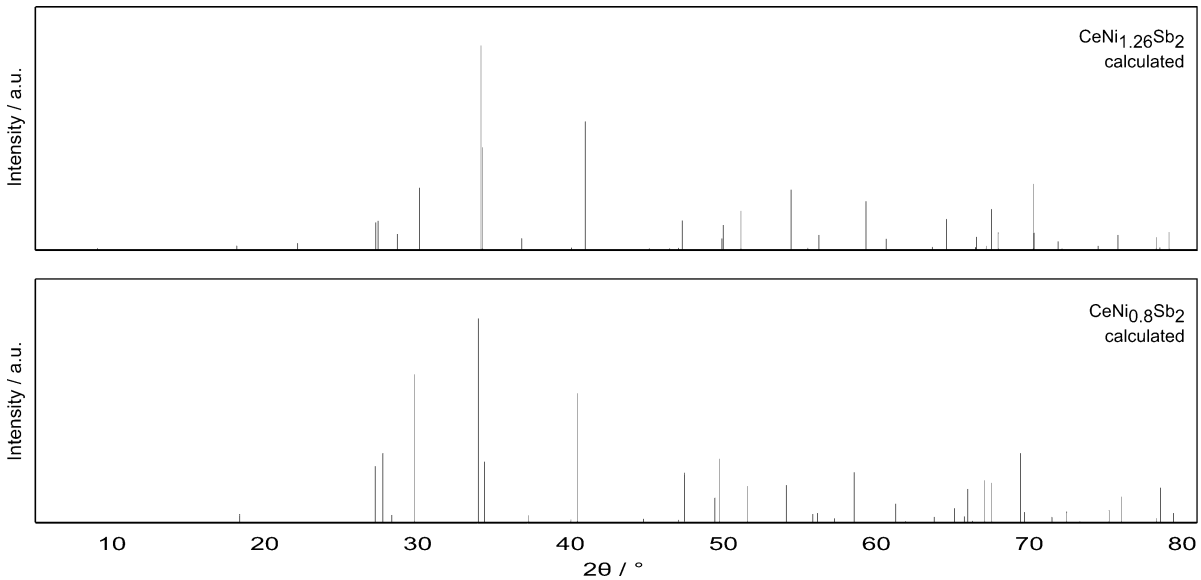

Fig. 3. Calculated powder patterns of $CeNi_{1.26}Sb_2$ and $CeNi_{0.8}Sb_2$ ($CuK_{\alpha 1}$ radiation).

First we discuss the course of the lattice parameters (Table 1). Two series of solid solutions have been investigated: (i) the series $CeNiSb_{1+y}Bi_{1-y}$ with fully occupied nickel sites and $CeNi_{1-x}Sb_{1+y}Bi_{1-y}$ with partially filled 2*b* positions. Substitution of antimony by the larger bismuth atoms leads to an almost Vegard-type increase of the *a* lattice parameter. In order to keep bonding with the neighboring layers, the *c* lattice parameter decreases, and thus the c/a ratio. The situation is more complicated for the samples with nickel defects. The variation in the *a* and *c* lattice parameters is not that pronounced, and the influence of structural disorder seems to dominate.

As emphasized in Fig. 2, the $CeNi_{1-x}Sb_{1+y}Bi_{1-y}$ structures exhibit layers of $NiSb_{4/4}$ tetrahedra where all tetrahedra share common edges. The Ni–Sb distances of 258 pm in $CeNiSb_{1.19}Bi_{0.81}$ are close to the sum of the covalent radii for nickel and antimony of 256 pm [38]. These tetrahedral layers correspond to the layers of condensed $FeAs_{4/4}$ tetrahedra in the pnictide oxide superconductor $LaFeAsO_{1-x}F_x$ [39]. The difference concerns the separating layer. In the classical pnictide oxides these separating layers consist of oxygen-centered rare earth tetrahedra, while in the $CeNi_{1-x}Sb_{1+y}Bi_{1-y}$ phases studied herein these layers show strong tetragonal distortions.

The bismuth/antimony atoms at $z = 0$ form square nets with Bi/Sb–Bi/Sb distances of 315 pm in $CeNiSb_{1.19}Bi_{0.81}$, only slightly longer than the two-electron two-center Bi–Bi bonds in the element (307 pm) [40]. In the second coordination sphere, these bismuth/antimony atoms are coordinated by four cerium atoms with Ce–Bi/Sb distances of 344 pm. These Ce–Bi/Sb contacts can only be considered as weak. The Ce–Bi/Sb distances are longer than in CeBi (325 pm) [41] and Ce_4Bi_3 (335 pm) [42]. The main bonding contribution for the cerium atoms results from the Ce–Ni contacts (318 pm Ce–Ni in $CeNiSb_{1.19}Bi_{0.81}$) with the neighboring layer.

The crystal chemical data of $CeNi_{1.26}Sb_2$ (Tables 1–4) were recorded for comparison. This antimonide has an additional nickel site which is inserted between the Sb2 square layers and the cerium atoms (Fig. 2). Together, the Sb2 and Ni1 atoms build up layers of edge-sharing tetrahedra, but one has to keep in mind that both nickel sites are only partially occupied, with the much lower occupancy for Ni1. The course of the interatomic distances is similar to that of the quaternary compounds (Table 4).

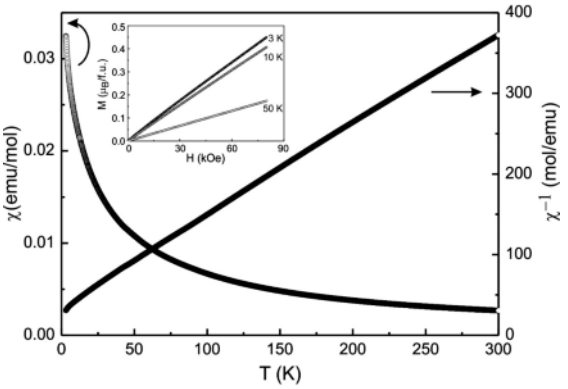

Fig. 4. Temperature dependence of the magnetic susceptibility (χ and χ^{-1} data) of CeNiSbBi measured at 10 kOe. The inset presents the magnetization isotherms at 3, 10 and 50 K.

The present investigation has clearly shown that the studied tetragonal phases have substantial phase width. Important features are nickel defects and/or the occupancy of an additional nickel site. These tiny differences can only be detected from precise single-crystal data. As a quintessence, a crystal may not be representative for a bulk sample!

Magnetic susceptibility measurements of CeNiSbBi

The temperature dependence of the susceptibility and inverse susceptibility (χ and χ^{-1} data), measured at an applied field of 10 kOe, is displayed in Fig. 4. A fit of the inverse susceptibility data in the investigated temperature range with a modified Curie–Weiss law ($\chi_m = C/(T - \Theta_p) + \chi_0$) yields an effective magnetic moment of $\mu_{eff} = 2.56(1)\,\mu_B$ per Ce atom. This is perfectly in line with the theoretical value of 2.54 μ_B for a free Ce^{3+} ion. Further fitting results are the Weiss-constant of $\Theta_p = -27(1)$ K and a temperature independent part of $\chi_0 = 1.7(1) \times 10^{-4}$ emu mol^{-1}. No magnetic ordering is evident down to 2.5 K, also at a lower applied field strength of 100 Oe (not shown here). Also no hint for a superconducting transition was observed. The inset presents the magnetization isotherms measured at 3, 10, and 50 K. All isotherms exhibit a linear increase of the magnetization with increasing field as expected for a paramagnetic material. The magnetization at 3 K and 80 kOe is 0.45(5) μ_B per Ce atom and is far below the theoretical value of 2.14 μ_B for Ce^{3+} (according to $g_J \times J$). Simi-

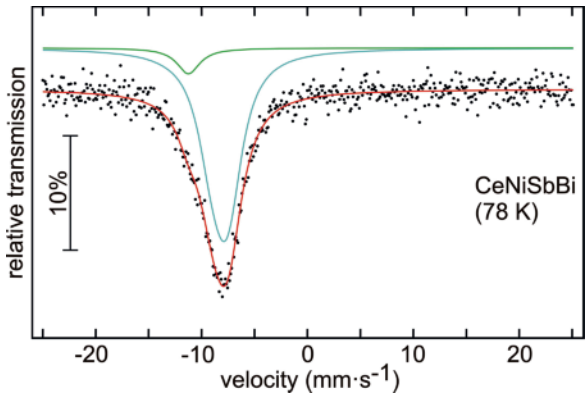

Fig. 5. (color online). Experimental (data points) and simulated (continuous lines) ^{121}Sb Mössbauer spectrum of the CeNiSbBi sample at 78 K.

lar magnetic behavior has been observed *e. g.* for $Ce_3Pd_4Sn_6$ [43] or CeAgMg [44].

^{121}Sb Mössbauer spectroscopy of CeNiSbBi

The ^{121}Sb Mössbauer spectrum of the CeNiSbBi sample at 78 K is presented in Fig. 5 together with a transmission integral fit. The spectrum could be well reproduced by a superposition of two spectral components. The main signal with 92(4) % corresponds to CeNiSbBi with an isomer shift of $\delta = -8.06(6)$ mm s^{-1}, subject to weak quadrupole splitting of $\Delta E_Q = -0.18(2)$ mm s^{-1}, a consequence of the non-cubic site symmetry 4*mm* of the antimony atoms. The experimental line width of $\Gamma = 3.2(1)$ mm s^{-1} is in the usual range for intermetallic antimony compounds. The isomer shift of CeNiSbBi is in good agreement with that of other antimonides, *e. g.* the series of the antimonides Yb*T*Sb (T = Ni, Cu, Pd, Ag, Pt, Au) [45], CeRhSb [5], or the antimonide oxides *RE*MnSbO and *RE*ZnSbO [46, 47], manifesting the antimonide character.

A small additional signal with 8(4) % was included in the fit with an isomer shift of $\delta = -11.2(4)$ mm s^{-1} and an experimental line width of $\Gamma = 2.6(9)$ mm s^{-1}. This small contribution corresponds to a minor Sb_2O_3 surface or grain boundary impurity that most likely resulted from the ceramic synthesis with repeated grinding. The experimental data for the Sb_2O_3 impurity are in excellent agreement with literature data [48, 49].

Acknowledgement

We thank Dipl.-Ing. Ute Ch. Rodewald for the intensity data collection and Janis Sälker for experimental help. This work was supported by the Deutsche Forschungsgemeinschaft.

[1] J.-L. Bobet, M. Pasturel, B. Chevalier, *Intermetallics* **2006**, *14*, 544.
[2] F. Weill, M. Pasturel, J.-L. Bobet, B. Chevalier, *J. Phys. Chem. Solids* **2006**, *67*, 1111.
[3] B. Chevalier, C. P. Sebastian, R. Pöttgen, *Solid State Sci.* **2006**, *8*, 1000.
[4] M. Pasturel, J.-L. Bobet, O. Isnard, B. Chevalier, *J. Alloys Compd.* **2004**, *384*, 39.
[5] B. Chevalier, R. Decourt, B. Heying, F. M. Schappacher, U.Ch. Rodewald, R.-D. Hoffmann, R. Pöttgen, R. Eger, A. Simon, *Chem. Mater.* **2007**, *19*, 28.
[6] V. K. Pecharskii, Y. V. Pankevich, O. I. Bodak, *Sov. Phys. Crystallogr.* **1983**, *28*, 97.
[7] L. Menon, S. K. Malik, *Phys. Rev. B* **1995**, *52*, 35.
[8] K. Hartjes, W. Jeitschko, *J. Alloys Compd.* **1995**, *226*, 81.
[9] L. Menon, S. K. Dhar, S. K. Malik, W. B. Yelon, *J. Appl. Phys.* **1996**, *79*, 6367.
[10] I. Karla, J. Pierre, R. V. Skolozdra, *J. Alloys Compd.* **1998**, *265*, 42.
[11] I. Karla, J. Pierre, B. Ouladdiaf, *Physica B* **1998**, *253*, 215.
[12] I. Karla, J. Pierre, A. P. Murani, M. Neumann, *Physica B* **1999**, *271*, 294.
[13] A. Ślebarski, E. D. Bauer, S. Li, M. B. Maple, A. Jezierski, *Phys. Rev. B* **2001**, *63*, 125126.
[14] M. G. Kanatzidis, R. Pöttgen, W. Jeitschko, *Angew. Chem. Int. Ed.* **2005**, *44*, 6996.
[15] U. Pfannenschmidt, U. Ch. Rodewald, R. Pöttgen, *Monatsh. Chem.* **2011**, *142*, 219.
[16] D. Voßwinkel, O. Niehaus, U. Ch. Rodewald, R. Pöttgen, *Z. Naturforsch.* **2012**, *67b*, 1241.
[17] Y. V. Pankevich, V. K. Pecharskii, O. I. Bodak, *Russ. Metall.* **1983**, *5*, 189.
[18] O. Sologub, K. Hiebl, P. Rogl, H. Noël, O. Bodak, *J. Alloys Compd.* **1994**, *210*, 153.
[19] Y. Muro, N. Takeda, M. Ishikawa, *J. Alloys Compd.* **1997**, *257*, 23.
[20] D. P. Gautreaux, M. Parent, A. B. Karki, D. P. Young, J. Y. Chan, *J. Phys. Condens. Matter* **2009**, *21*, 056006.

[21] W. K. Hofmann, W. Jeitschko, *J. Less-Common Met.* **1988**, *138*, 313.
[22] H. Flandorfer, O. Sologub, C. Godart, K. Hiebl, A. Leithe-Jasper, P. Rogl, H. Noël, *Solid State Commun.* **1996**, *97*, 561.
[23] H. Mizoguchi, S. Matsuishi, M. Hirano, M. Tachibana, E. Takayama-Muromachi, H. Kawaji, H. Hosono, *Phys. Rev. Lett.* **2011**, *106*, 057002.
[24] K. Kodama, S. Wakimoto, N. Igawa, S. Shamoto, H. Mizoguchi, H. Hosono, *Phys. Rev. B* **2011**, *83*, 214512.
[25] A. Buckow, K. Kupka, R. Retzlaff, J. Kurian, L. Alff, *Appl. Phys. Lett.* **2012**, *101*, 162602.
[26] K. Yvon, W. Jeitschko, E. Parthé, *J. Appl. Crystallogr.* **1977**, *10*, 73.
[27] V. Johnson, W. Jeitschko, *J. Solid State Chem.* **1974**, *11*, 161.
[28] L. Palatinus, G. Chapuis, *J. Appl. Crystallogr.* **2007**, *40*, 786.
[29] V. Petříček, M. Dušek, L. Palatinus, JANA2006, The Crystallographic Computing System, Institute of Physics, University of Prague, Prague (Czech Republic) **2006**.
[30] R. A. Brand, NORMOS, Mössbauer Fitting Program, Universität Duisburg, Duisburg (Germany) **2007**.
[31] H . Sprenger, *J. Less-Common Met.* **1974**, *34*, 39.
[32] L. S. Andruchiv, L. O. Lysenko, Ya. P. Yarmolyuk, E. I. Gladyshevskii, *Dopov. Akad. Nauk. Ukr., Ser. A* **1975**, 645.
[33] R. Pöttgen, D. Johrendt, *Z. Naturforsch.* **2008**, *63b*, 1135.
[34] D. C. Johnston, *Adv. Phys.* **2010**, *59*, 803.
[35] D. Johrendt, H. Hosono, R.-D. Hoffmann, R. Pöttgen, *Z. Kristallogr.* **2011**, *226*, 435.
[36] E. Parthé, L. M. Gelato, *Acta Crystallogr.* **1984**, *A40*, 169.
[37] L. M. Gelato, E. Parthé, *J. Appl. Crystallogr.* **1987**, *20*, 139.
[38] J. Emsley, *The Elements*, Oxford University Press, Oxford **1999**.
[39] Y. Kamihara, T. Watanabe, M. Hirano, H. Hosono, *J. Am. Chem. Soc.* **2008**, *130*, 3296.
[40] J. Donohue, *The Structures of the Elements,* Wiley, New York **1974**.
[41] G. L. Olcese, *Atti Accad. Naz. Lincei, Cl. Sci. Fiz., Mat. Nat. Rend.* **1966**, *40*, 629.
[42] D. Hohnke, E. Parthé, *Acta Crystallogr.* **1966**, *21*, 435.
[43] D. Niepmann, R. Pöttgen, B. Künnen, G. Kotzyba, B. D. Mosel, *Chem. Mater.* **2000**, *12*, 533.
[44] D. Johrendt, G. Kotzyba, H. Trill, B. D. Mosel, H. Eckert, Th. Fickenscher, R. Pöttgen, *J. Solid State Chem.* **2002**, *164*, 201.
[45] R. Mishra, R. Pöttgen, R.-D. Hoffmann, Th. Fickenscher, M. Eschen, H. Trill, B. D. Mosel, *Z. Naturforsch.* **2002**, *57b*, 1215.
[46] I. Schellenberg, H. Lincke, W. Hermes, V. Dittrich, R. Glaum, M. H. Möller, R. Pöttgen, *Z. Naturforsch.* **2010**, *65b*, 1191.
[47] I. Schellenberg, T. Nilges, R. Pöttgen, *Z. Naturforsch.* **2008**, *63b*, 834.
[48] G. G. Long, G. J. Stevens, L. H. Bowen, *Inorg. Nucl. Chem. Lett.* **1969**, *5*, 799.
[49] P. E. Lippens, *Solid State Commun.* **2000**, *113*, 399.